Supplementary Information for

Digital phase-shift mask projection lithography enabling sub-diffraction-limit resolution for dense nanoscale patterning

Yuan-Yuan Zhao[1,2,3,*], Zi-Xin Liang[1,2,3], Jing-Tao Chen[1,2,3], Wen-Hui Li[1,2], Zhi-Cai Wu[1,2], and Xuan-Ming Duan[1,2,*]

[1] Guangdong Provincial Key Laboratory of Optical Fiber Sensing and Communications, Institute of Photonics Technology, Jinan University, Guangzhou 511443, China

[2] College of Physics & Optoelectronic Engineering, Jinan University, Guangzhou 510632, China

[3] Those authors have equal contributions to this work.

[*] Authors to whom any correspondence should be addressed.

E-mail: yyzhao@jnu.edu.cn and xmduan@jnu.edu.cn

Supplementary Note 1. Experimental system of PSM-DPL

The detailed programmed phase-shift mask digital projection nanolithography (PSM-DPL) system is shown in Figure S1. In this system, a homogenized femtosecond pulse laser with a center wavelength of 517 nm, a repetition frequency of 10 MHz, and a pulse width of ~240 fs is combined with an amplitude-type LCOS-SLM and phase-type LCOS-SLM cascade system, which is customized for the patterning process. Spatial light field distribution. The amplitude-type LCOS-SLM and phase-type LCOS-SLM used in this system are composed of 1080 × 1920 single pixels, and the single pixel size is 8 μm. Computer-related software can be loaded into two modulators with 0 to 255 grayscale images to control the exposure light field. The composite modulated light field real-time monitoring unit can independently detect the target light field amplitude and phase information. Close the 5:95 beam splitter prism (BS) lower diaphragm to achieve pure amplitude modulation. The amplitude-modulated light without phase modulation reaches the CMOS through the phase delay line composed of a 50:50 BS and an imaging amplification system to realize the detection of light field intensity distribution. When the diaphragm is opened, coherent amplitude-only modulated light and composite modulated light interfere at the BS in front of the CMOS, and the interference fringes received by the CMOS reflect the corresponding phase information. The exposed sample is placed on an automatic *x*-, *y*- and *z*-axis electric translation stage (AG10010H, OptoSigma), which can move axially with a minimum step size of 1 μm in the *x*/*y* direction and 0.1 μm in the *z* direction to achieve multi-region processing of the sample.

Table S1 Spatial light modulator parameter list

	Amplitude type LCOS-SLM	**Phase type LCOS-SLM**
Model	HED-6001	PLUTO-2-UV-099
Material	Reflective liquid crystal on silicon	Reflective liquid crystal on silicon
Gray level	8-bit (Level 256)	8-bit (Level 256)
Dynamic range	>1000:1	——
Phase range	——	>2π@405nm; >π@532nm;
Effective area	15.36 mm×8.64 mm	15.36 mm×8.64 mm

Resolution	1920×1080	1920×1080
Pixel size	8 μm	8 μm
Fill factor	87%	93%
Diffraction efficiency	> 60%	> 90% (Average)
Frame rate	60 Hz	60 Hz
Damage threshold	~ 2 W/cm²	~ 2 W/cm²

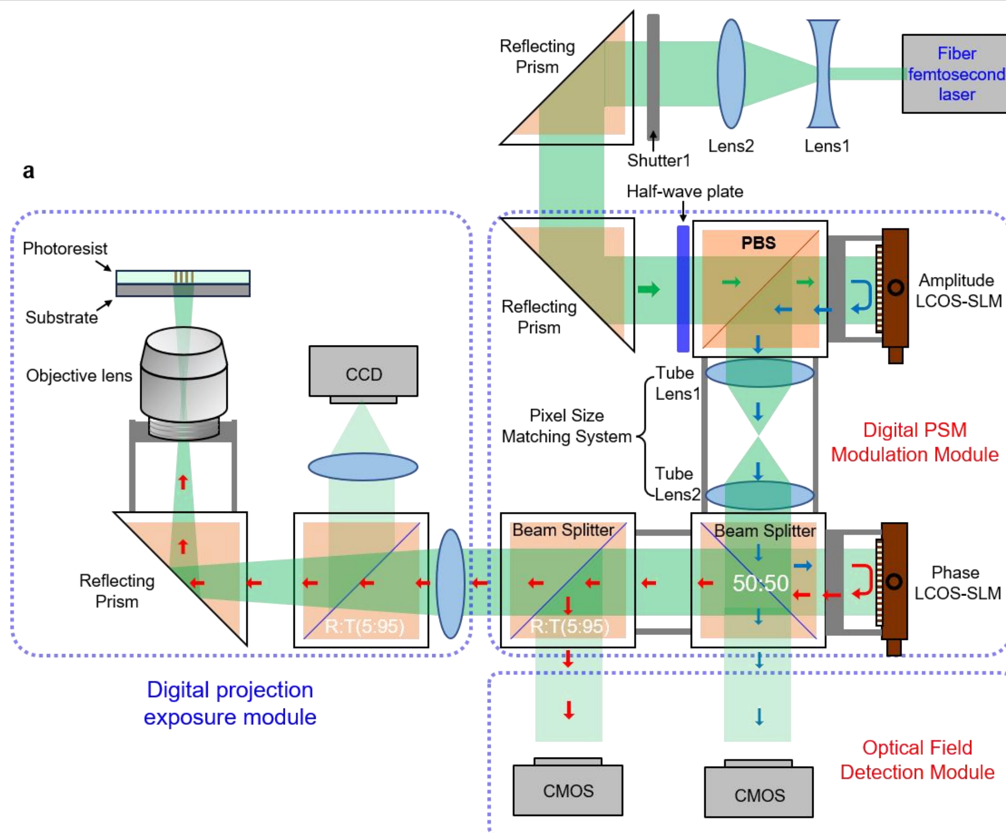

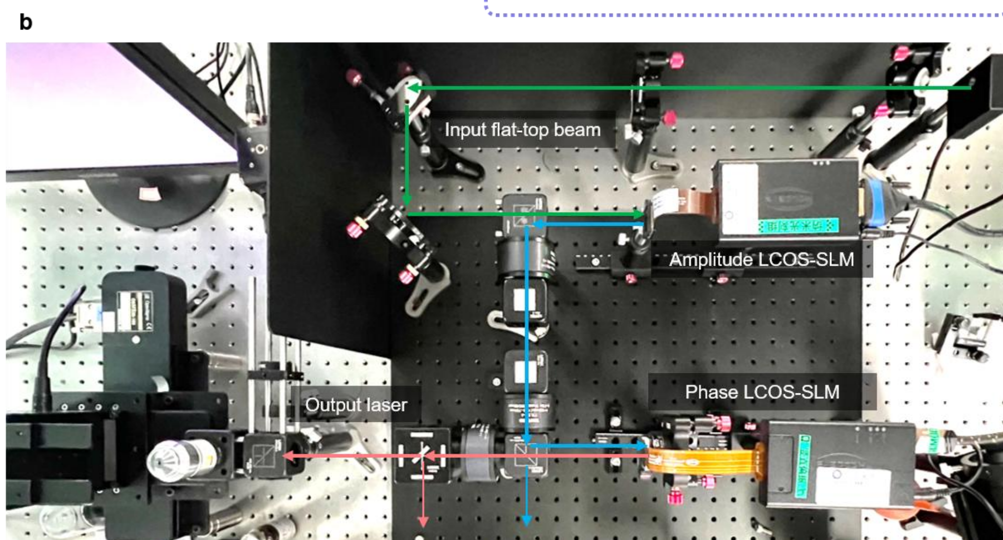

Figure S1 (a) Amplitude and phase composite modulation light field exposure unit, and Light field real-time monitoring unit. (b) Light path diagram of the actual built system.

To achieve pixel-level alignment between the two SLMs shown in Figure S1(a), in addition to a 1:1 4F imaging system, one of the LCOS-SLMs (a phase-type LCOS-SLM in our setup) is mounted on a six-axis adjustment stage (LBTEK, AMM6-1A). This configuration allows spatial positioning in three dimensions, ensuring both the convenience and practicality of precise pixel alignment. The primary objective of this alignment procedure is to achieve integer-pixel registration, which is critical for executing high-fidelity phase-shifting mask (PSM) lithography. In this context, sub-pixel translational misalignments and rotational offsets between the two SLMs are the main factors that can compromise the accuracy of complex amplitude modulation. As illustrated in Figure S2(a), the pixel array of the phase-type LCOS-SLM can be displaced relative to that of the amplitude-type LCOS-SLM along the ΔX and ΔY directions and adjusted in terms of tilt angles $\Delta\theta_x$ and $\Delta\theta_y$, as well as an in-plane rotational angle α within the XY plane.

To mitigate the effects of residual sub-pixel or rotational misalignments, our system employs real-time monitoring of the optical field and reference features, which allows precise measurement of these deviations. The measured offsets are then fed back to the six-axis stage, which, in combination with the 4F optical relay, ensures accurate pixel-level registration of the two SLMs. By combining multiple degrees of adjustment and active feedback, the dual-SLM system maintains the necessary alignment precision for high-resolution PSM-DPL exposures. Figure S2(b) shows a photograph of the six-axis adjustment stage in the assembled system, illustrating the practical implementation of this pixel-level alignment strategy, which effectively mitigates the detrimental effects of both sub-pixel and rotational misalignments and ensures robust, high-fidelity lithographic performance.

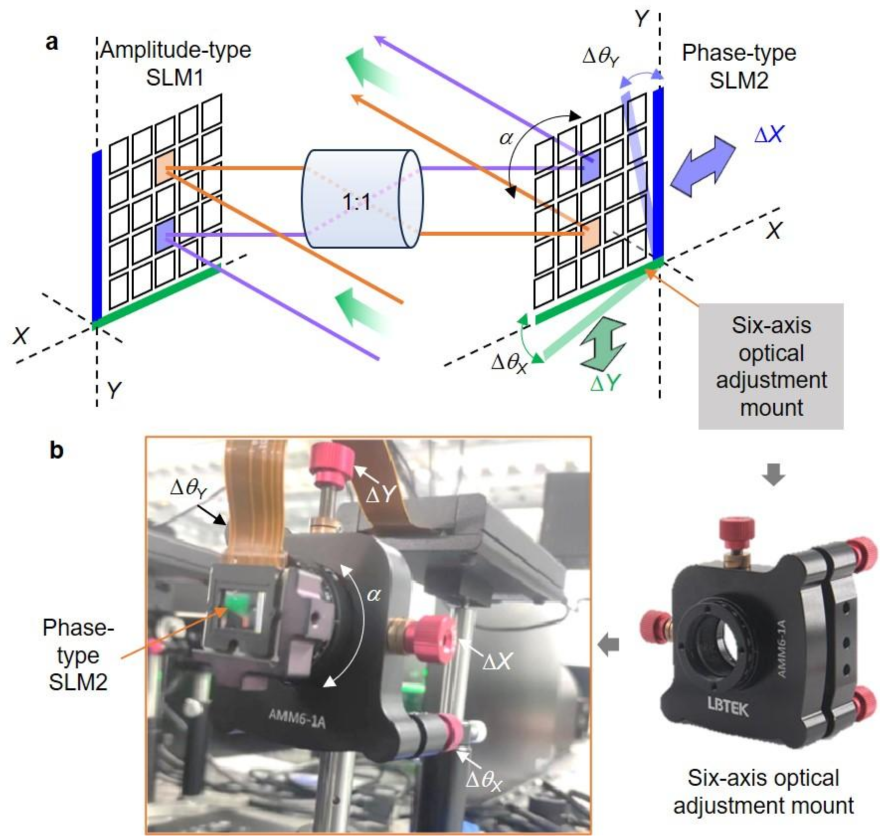

Figure S2 (a) Schematic diagram of pixel matching and alignment adjustment system. (b) Actual photos of six-axis optical adjustment mount.

Supplementary Note 2. Amplitude and phase modulation correction of LCOS-SLM

The LCOS-SLM used in the system is all 256-grayscale modulation. This system uses a 517 nm femtosecond laser light source. It is easy to know that under different wavelength light source conditions, the grayscale modulation curve of the LCOS-SLM is quite different. In order to obtain accurate amplitude and phase grayscale masks and recommend the correct simulation model, it is necessary to measure the grayscale curves of the two LCOS-SLMs separately.

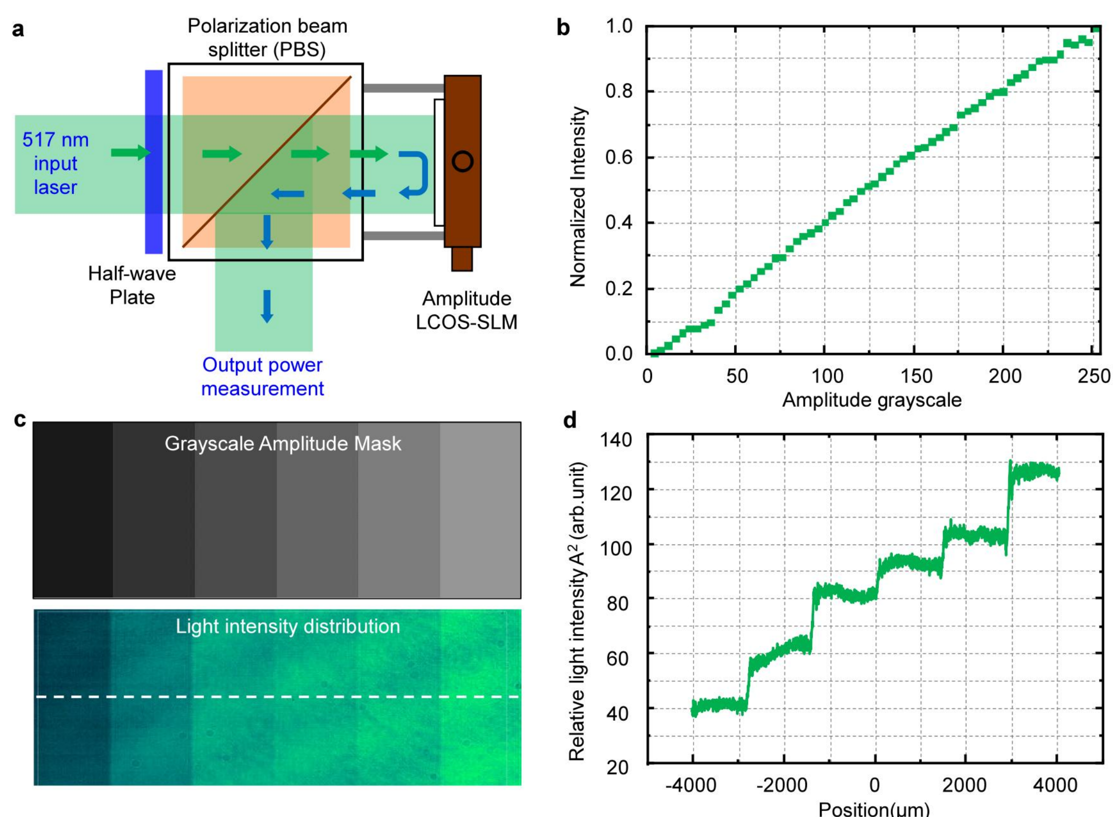

Figure S3 (a) Amplitude-type LCOS-SLM measurement optical path diagram; (b) Normalized grayscale intensity curve of the amplitude-type LCOS-SLM loaded with different amplitude grayscale values; (c) Amplitude-type LCOS-SLM loaded with 6 grayscale amplitude step distribution masks, and 2D light intensity distribution; (d) Light intensity distribution contour diagram at the cross section in Figure c.

Figure S3(a) is a typical amplitude-type LCOS-SLM (Holoeye, HED-6001) measurement optical path. The femtosecond laser is converted into polarized light (parallel to the short axis of the target surface) required by the complex amplitude-type

LCOS-SLM through a half-wave plate and reaches the amplitude-type LCOS-SLM through the PBS to achieve amplitude modulation. After that, the light field is output through the PBS, and the optical path is measured. The modulation principle of the amplitude-type LCOS-SLM is to change the polarization degree of the output light. The PBS plays the role of polarization and polarization analysis and realizes light intensity modulation based on Malus's law. The normal incident measurement optical path effectively limits the measurement deviation. The LCOS-SLM loads the full target surface image of 0 ~ 255 grayscale in sequence. After 4 measurements, the normalized grayscale intensity curve in Figure S3(b) is obtained. It can be seen that the LCOS-SLM amplitude grayscale modulation curve used by the system has good linearity (Figure S3(c-d)). Grayscale can be understood as the transmittance of the transmissive mask, which provides data support for the establishment of grayscale complex amplitude light field simulation.

The phase-type LCOS-SLM (Holoeye, PLUTO-2-UV-099) used in this system can achieve a phase modulation range of 2.3π at a wavelength of 405 nm. Theoretically, to achieve a complex amplitude light field with the largest possible modulation range, the phase modulation range must be $\geq \pi$. The methods of phase detection and calibration mainly include interferometry and diffraction measurement. Among them, the interferometry method is widely used due to its high measurement accuracy. This paper adopts the self-reference calibration method in the interferometry method. From the literal meaning, it is not difficult to understand that this method divides the target surface into a modulation area and a reference area, so that the light in the two areas interferes to calibrate the phase. The measurement optical path of the phase-type LCOS-SLM constructed under a 517 nm femtosecond laser is shown in Figure S4(a).

The expanded beam passes through a half-wave plate (HWP), a polarizer, and a 50:50 beam splitter (BS) before reaching the phase-only LCOS-SLM surface. The HWP and polarizer ensure that the incident polarized light's direction aligns as closely as possible with the liquid crystal molecules' orientation, maximizing the interference fringe contrast. On the LCOS-SLM surface, half of the area is loaded with a uniform grayscale value, while the other half is patterned with a binary grating structure composed of

alternating 0 and grayscale values, shown in Figure S4(c). This grating functions as a diffractive optical element (DOE), causing the 0th-order beam to propagate along the optical axis while diffracting higher-order beams at specific angles relative to the axis.

$$E_5 = A_0(x, y)\mathrm{e}^{j\varphi(x,y)}\begin{bmatrix} 0 \\ -\sin\theta \end{bmatrix} \tag{S1}$$

Here, m denotes the diffraction order, λ the incident light wavelength, and Λ the grating period. The region with a uniform grayscale value serves as a reflective area, functioning as a mirror that propagates light along the optical axis. This reflected light interferes with the diffracted light from the grating, generating interference fringes.

Theoretically, the interference fringes exhibit the highest contrast when the grating's grayscale gradient corresponds to a π-phase shift. However, under a 517 nm light source, the exact grayscale value required for a π-phase shift is unknown and must be experimentally determined by varying the grating's grayscale while observing the resulting fringes. Ultimately, a binary diffraction grating with alternating 0 and 160 grayscale values and a 4-pixel period was selected. A laser beam expander was placed before the 50:50 beam splitter (BS) to allow direct visual alignment, ensuring that the reflected light overlapped only with the first-order diffracted beam while maximizing the interference area. Once optimized, the beam expander was removed, and a CMOS camera was positioned to capture the interference patterns.

For phase calibration of the LCOS-SLM, the grating region remained unchanged, while the reflective region's grayscale varied from 0 to 255 in steps of 5. By analyzing the fringe displacement in the captured interference patterns, the phase shift could be determined. The relationship between phase change and positional shift is given by:

$$\phi = \frac{2\pi}{P} \cdot \delta d \tag{S2}$$

Here, δd represents the relative displacement of the interference fringes, and P denotes the measured fringe period. The constructed measurement system not only enables the determination of the global grayscale-phase relationship but also facilitates the assessment of grayscale-phase nonuniformity across the SLM surface.

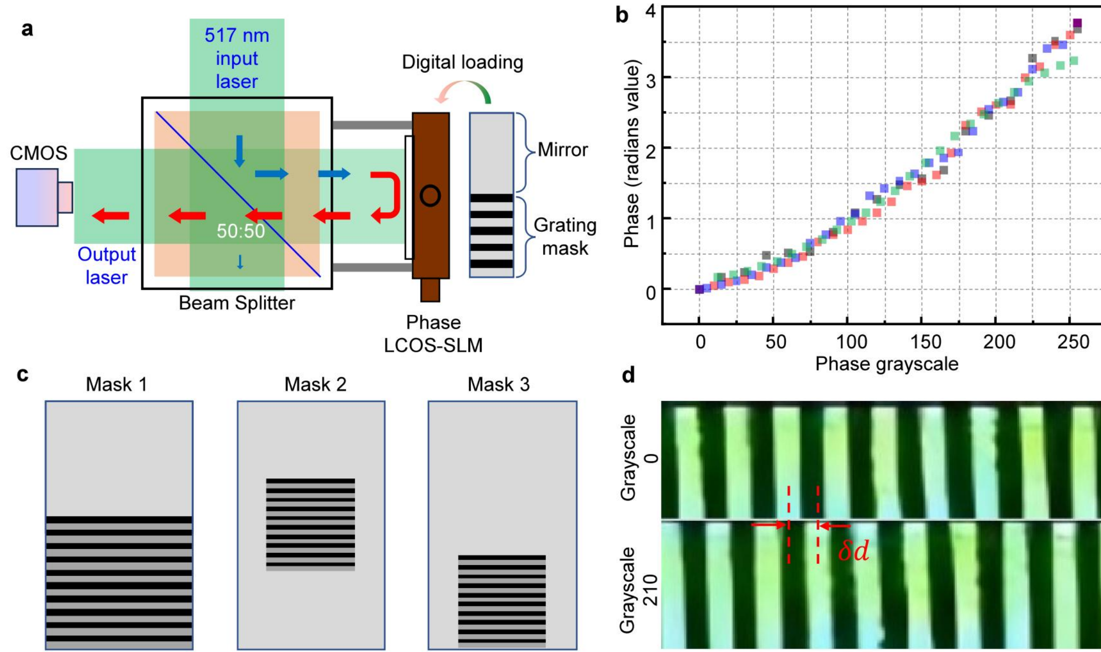

Figure S4 (a) Phase measurement optical path diagram of phase-type LCOS-SLM; (b) Measured phase grayscale modulation curve; (c) Loading diagram corresponding to phase global calibration, center calibration and edge calibration; (d) Relative displacement of interference fringes generated by 0 grayscale and 210 grayscales.

During the actual measurements, in addition to the half-reflective region (uniform grayscale) and half-diffractive grating region, two additional calibration patterns (Figure S4(c), mask2 and mask3) were employed to perform global phase measurement, central region measurement, and edge region measurement. The results of these three measurements are presented in Figure S4(b), demonstrating excellent linearity in the grayscale-phase response curve. As illustrated in Figure S4(d), when the reflective region was set to 0 grayscale and 210 grayscales, respectively, the observed fringe shift approached half a period, corresponding to a π-phase shift. This confirms that a grayscale value of 210 induces a π-phase modulation, which is consistent with the grayscale-phase modulation curve shown in Figure S4(b).

Supplementary Note 3. Comparison of composite modulated light field solutions

Spatial light modulators (SLMs) are a critical tool for modulating the amplitude and phase of optical fields, and have been widely applied in microscopy, detection, laser communication, and laser processing. Conventional SLMs typically modulate only a single parameter of the light field—either amplitude or phase—spatially. Some studies have employed a single SLM based on the super-pixel principle or dual phase-only SLMs to achieve composite amplitude-phase modulation (see Table S2). However, these approaches sacrifice pixel count to gain degrees of freedom in spatial light field modulation, making it difficult to meet the demands of ultra-high-density pixels and large-area spatiotemporal photon modulation.

In particular, digital mask projection lithography commonly utilizes DMDs (digital micromirror devices) or LCOS-SLMs (liquid crystal spatial light modulators) as light-field modulation components to generate programmable "digital masks," enabling arbitrary-pattern light fields for photoresist exposure. However, due to the limited degrees of freedom in modulation—typically restricted to either amplitude or phase—the topological optimization of the light field is constrained, resulting in lower lithographic resolution. Thus, achieving higher-resolution and higher-fidelity fine structures require smaller pixel sizes and a larger number of pixels working in coordination.

Our proposed dual-SLM cascaded modulation scheme offers the following advantages: *1. True independent modulation of amplitude and phase; 2. Vertical illumination, facilitating projection micro-imaging; 3. Real-time monitoring of dynamically modulated light fields; 4. Specifically tailored for lithography applications (large target surface, small pixel size).* We compare this scheme with other light-field modulation methods and present a radar chart for reference (Figure S5).

Table S2 Complex amplitude modulation strategy

Year/Group	Modulation method	Modulator type	Advantages and Disadvantages

[1]	1992/ Gregory's Group	Two LCD screens are cascaded to control the light field through the 4F system	Transmissive LCD screen, the optical axis is parallel to the normal line of the LCD screen	• Pixelated independent modulation; • Low optical resolution; • Low modulation efficiency.
[2]	2008/ Van Putten's Group	Single-phase SLM modulates the light field through a 4-in-1 "super pixel" combination	Reflective phase type LCOS-SLM, the optical axis is parallel to the normal	• Amplitude and phase are not completely independently modulated; • Low pixel resolution.
[3]	2014/ Goorden's Group	A single DMD controls the light field by combining "super pixels" and spatial filtering technology	Reflective DMD, the emitted light field is parallel to the normal direction	• Amplitude and phase can be independently modulated in single super pixel; • Low resolution ; • Extremely low light energy utilization.
[4]	2013/ Han's Group	Two phase-type SLMs, each SLM is half-side modulated, and the light field is controlled through the 4F system cascade	Reflective phase type LCOS-SLM, the optical axis is parallel to the normal line	• Amplitude and phase are independently modulated; • The structure is compact and the pixel alignment is difficult to control; • There is large aberration. • Low resolution. • The amplitude is controlled by the polarization state, and the light energy utilization rate is low.
[5]	2014/ Zhu's Group	Two phase-type SLMs are cascaded to control the light field through the 4F system	Reflective phase type LCOS-SLM, the optical axis is tilted from the normal line	• Amplitude and phase are independently modulated; • Large aberration exists during surface projection; • High resolution and high light energy utilization
[6]	2016/ Leportier's Group	Two amplitude types are independently adjusted, plus PBS, $\lambda/4$ wave plate and 45° linear polarizer to modulate the complex amplitude light field	Reflective amplitude type LCOS-SLM, the optical axis is parallel to the normal line	• Amplitude and phase are independently modulated; • The structure is simple; • Energy in one polarization direction will be lost through PBS, and the light energy utilization rate is low.
[7]	2025/ Our Group	Amplitude type SLM + phase type SLM are cascaded through the 4F system	Reflective SLM, the optical axis is perpendicular to the SLM screen	• True independent modulation of amplitude and phase; • Vertical illumination, convenient for projection micro-imaging; • Real-time monitoring (scientific research users); • As required for photolithography applications (large target surface, small pixel)

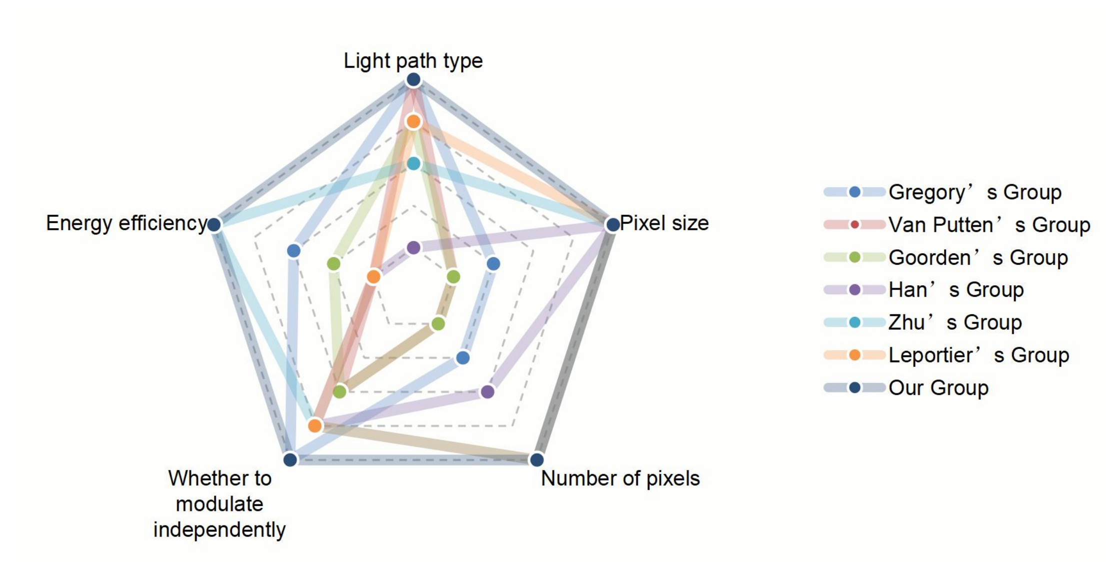

Figure S5 Radar diagram of advantages and disadvantages of different composite light field modulation technologies.

Supplementary Note 4. Pixel size matching and position alignment technology of cascaded dual SLM

In the optical configuration shown in Figure 2 or Figure S2(a), the pattern generated by the amplitude-type SLM is imaged onto the modulation plane of the phase-type SLM via a 4F imaging system. Since both SLMs have identical pixel sizes and arrangements, Lens 1 and Lens 2 are designed with equal focal lengths. As indicated in Figure 2, the image formed on the phase-type SLM is an inverted version of the original amplitude pattern. Therefore, this 1:1 object-image correspondence must be taken into account when loading grayscale images onto the two SLMs. To achieve precise optical field control, corresponding grayscale patterns must be loaded onto both SLMs to independently modulate amplitude and phase. The degree of alignment between the amplitude and phase information generated by the two SLMs directly determines the accuracy of the final optical field modulation. To facilitate the precise positioning of the SLMs, a six-axis optical adjustment stage (Figure S2(b)) is used to mount the modulator surface. This adjustment stage allows translational motion along three axes, tilt control, and full 360° rotation, enabling fine alignment of the optical components.

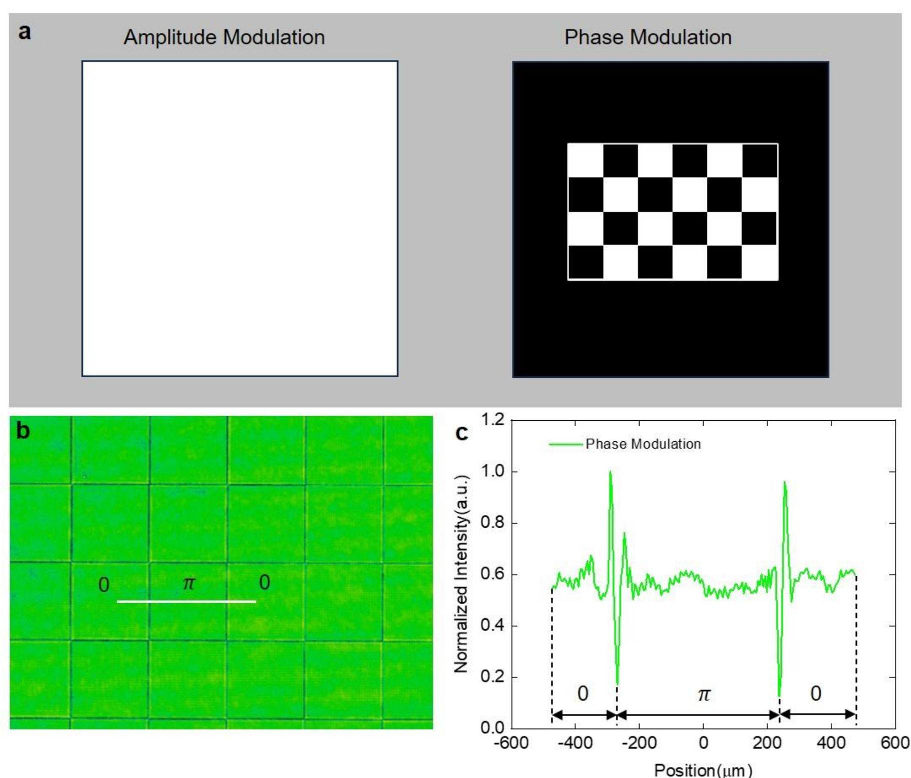

Figure S6 (a) Digitally loaded mask for pure phase-modulated optical field experiments; (b) Captured image of a 64-pixel black-and-white checkerboard pattern generated via pure phase modulation; (c) Corresponding loaded patterns for global, central, and edge-region phase calibration; (d) Cross-sectional intensity profile along the marked line in (b).

Phase-only modulation of the optical field can also generate patterns. However, unlike amplitude modulation, which directly alters light intensity, phase modulation solely changes the phase of the optical field without affecting its intensity. Nevertheless, at locations with phase conflicts, destructive interference occurs, resulting in localized intensity minima (dark regions), while the intensity in other areas remains unchanged. This leads to the formation of patterns with contrast between bright and dark regions. To investigate the relationship between phase modulation and resolution, we configured the phase-type LCOS-SLM to load various phase patterns, while the amplitude-type LCOS-SLM was loaded with a uniform grayscale value of 255. This configuration is referred to as phase-only modulation, as illustrated in Figure S6(a).

Figure S6b shows the captured optical field image when the phase-type LCOS-SLM is loaded with a 64-pixel black-and-white checkerboard pattern. The detected intensity at the position of maximum signal on the detector is defined as the unit intensity, and all input intensities are normalized accordingly. As illustrated in Figures S6a and S6b, a sharp intensity variation occurs at the phase transition boundaries between black (phase 0) and white (phase π) regions. Due to destructive interference between adjacent optical fields, the modulated optical field exhibits intensity minimum at the boundaries of the phase transition (from 0 to π), where phase conflicts occur. In contrast, the intensity remains nearly uniform across other regions, resembling a collimated light field distribution. At the phase discontinuities, the intensity drops to a clear minimum (forming a distinct valley). In Figure S6c, the measured width corresponding to the π phase region is 505 μm, which is in good agreement with the theoretical width of 512 μm.

Due to the small pixel size of the LCOS-SLMs, it is not feasible to directly measure the positional offset between corresponding pixels on the two SLMs. Therefore, pixel-level alignment is typically achieved by loading specially designed alignment masks onto both modulators and analyzing the resulting optical field captured by a beam quality analyzer.

The amplitude mask is designed as a grid pattern composed of two-pixel-wide lines, as shown in Figure S7(a). The corresponding optical field exhibits a grid-like intensity distribution, as shown in Figure S7(b). The phase mask used for alignment is shown in Figure S7(c), designed as a checkerboard pattern in which adjacent pixels represent phase values of 0 and π, respectively. The abrupt phase change between neighboring pixels (from 0 to π) causes destructive interference, resulting in dark-field regions. This yields a grid-like dark-line pattern in the optical field, as shown in Figure S7(d), which corresponds one-to-one with the bright-line grid pattern produced by amplitude modulation.

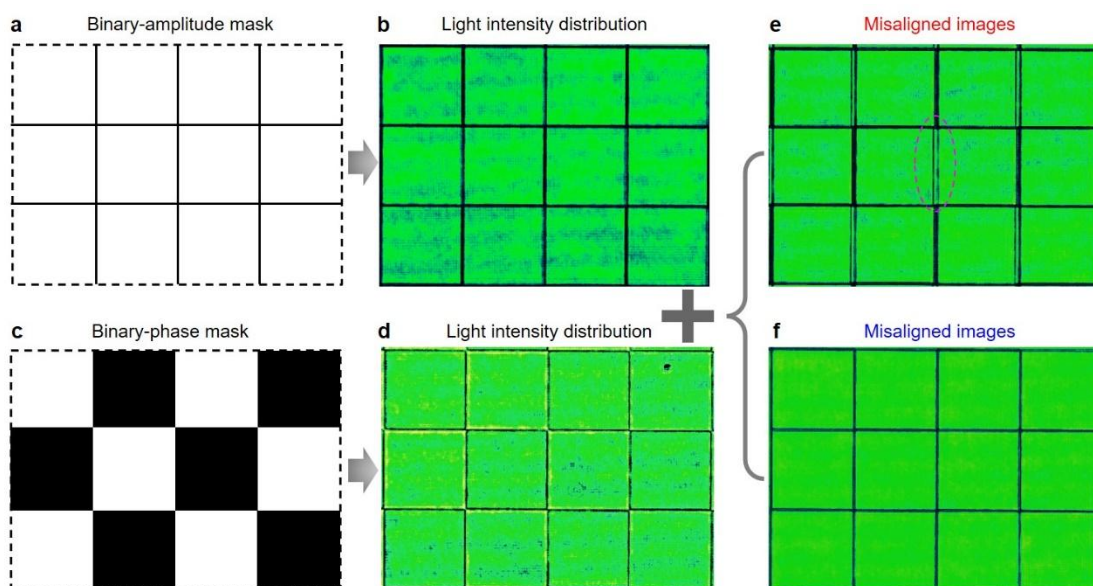

Figure S7 Pixel-level alignment between the amplitude-type and phase-type LCOS-SLMs: (a) A pure amplitude “digital mask”; (b) the corresponding optical field distribution under pure amplitude modulation; (c) A pure phase “digital mask” ; (d) the resulting optical field distribution under pure phase modulation. (e) the optical field captured under dual modulation when the two SLMs are misaligned, and (f) the optical field distribution after pixel-level alignment of the two SLMs.

By adjusting the six-axis optical adjustment stage (Figure S2(b)), pixel-level alignment of the two SLMs can be achieved. Figures S7(e) and S7(f) show the optical fields captured using a beam quality analyzer before and after alignment, respectively. When the horizontal and vertical grid lines appear split into two distinct lines, it indicates that the SLMs are misaligned. When these lines merge into single lines, it confirms that pixel-level alignment has been successfully achieved.

Supplementary Note 5. Modeling of complex amplitude modulation projection imaging system

In this system, the LCOS-SLM target surface is composed of a pixel array. A single pixel of the amplitude-type LC-SLM can be regarded as a rectangular hole with adjustable transmittance, and a phase-type LCOS-SLM can be regarded as a rectangular hole with different thicknesses, that is, different optical path differences are introduced, thereby carrying different phase information. The distribution size of the complex amplitude on the image plane corresponds linearly to the digital mask. The complex amplitude distribution of the light field is combined with the photoresist threshold model, which ultimately affects the lithography pattern morphology.

The light generated by a single pixel as a light source can be regarded as an ideal Gaussian beam diffracted according to the Fraunhofer moment hole. The complex amplitude of the pixel point (x, y) in the vector form on the rear focal plane of the objective lens can be expressed according to the series of Literature. The light intensity distribution function after loading the DMD digital mask was obtained. $h(x,y)$ represents the PSF in a certain polarization direction, * is the convolution operation, and I is the projected light intensity distribution.

$$I(x,y)=\sum|h(x,y)*[m_1(x,y)*m_2(x,y)]|^2 \tag{S3}$$

Where $m_1(x, y)$ represents the complex amplitude transmittance function of the amplitude-type LCOS-SLM, and $m_2(x, y)$ represents the complex amplitude transmittance function of the phase-type LCOS-SLM.

$$m_1(x,y)=\sum\nolimits_{i\,j} a_{(i,j)}u_{i,\,j}(x,y) \tag{S4}$$

$$m_2(x,y)=\sum\nolimits_{i,j} \exp\left[i\varphi_{i,\,j}(x,y)\right] \tag{S5}$$

Among them, $u_{i,j}(x,y)$ is a rectangular function, $a_{i,j}(x,y)$ can represent different transmittance coefficients. The normalized grayscale intensity measured in Figure S4(b) is used to realize the distribution of different grayscale digital masks and different light field intensities. $\varphi_{i,\,j}(x,y)$ represents the phase value loaded by the pixel. Based on the phase-type LCOS-SLM used in the complex amplitude modulation system, the phase

value loaded by the pixel corresponds to the phase grayscale value and can also be regarded as a function of the grayscale value. The grayscale phase relationship measured in Figure S5(b) is used to realize grayscale phase call.

$$a_{i,j}(x,y) = f_1(grayscale) \tag{S6}$$

$$u_{(i,j)}(x,y) = \mathrm{rect}\left[\frac{x}{w_x} - iT_x, \frac{y}{w_y} - jT_y\right] \tag{S7}$$

$$\varphi_{i,j}(x,y) = f_2(grayscale) \tag{S8}$$

Where T_x and T_y are the size of the bright field distribution of the mask in the *X* and *Y* directions, w_x and w_y are the length and width of a single pixel, *h*(*x*,*y*) is the system point spread function, *i* and *j* represent the position of the pixel in the mask pixel array, and * represents the convolution operation. Based on this, the superimposed light field distribution generated by the joint action of multiple pixels is:

$$I = \left|\sum\nolimits_{ij} h(x,y) * a_{(i,j)} u_{i,j}(x,y) * \exp\left[\varphi_{i,j}(x,y)\right]\right|^2 \tag{S9}$$

It can be seen from the formula that the amplitude and phase information of the system's projected light field can be independently controlled at the level of a single pixel. Therefore, the implemented complex amplitude modulation method has the advantages of a high degree of freedom, independent and direct control of amplitude and phase, and independent control of a single pixel.

Supplementary Note 6. Sparrow criterion for the line periodic resolution

In our manuscript, we employ a parallel lithography system based on digital mask projection, as illustrated in Figure S8(a). The previously discussed two-photon Sparrow criterion is applicable only to serial lithography; thus, we must now address the Sparrow criterion in the context of parallel lithography, which is analogous to traditional projection lithography using physical masks [7-9]. In projection imaging systems, the Sparrow criterion is established based on the condition that the optical system's modulation transfer function (MTF) equals zero [7,10]. When the line periodic resolution reaches the value defined by the Sparrow criterion, the corresponding MTF condition allows for a resolvable image in the photoresist [10]. Under axial point source illumination, the cutoff frequency of the projection optical system is defined as NA/λ (where the +1 or -1 diffraction orders are situated at the edge of the entrance pupil), leading to a theoretical resolution of d=λ/NA for lithographic imaging [11].

For single-photon exposure, the coherent linear superposition of light intensity from parallel exposure results in a local minimum appearing precisely at the center, with the exposure dose distribution of the adjacent projection light fields (proportional to intensity I) being resolvable, as shown in Figure S8 (b,d). Even with two-photon exposure, the resolvable pitch for the exposure dose between adjacent projection light fields remains at the critical value of d=λ/NA, constrained by the minimum spacing resulting from the superposition of adjacent light intensities; the exposure dose is simply proportional to I^2. Thus, d=λ/NA represents “the general Sparrow criterion” for parallel projection lithography.

When employing off-axis point source illumination, such as through oblique illumination [9,12] or equivalent phase-shifting masks [9,13], the cutoff frequency of the projection optical system increases to 2NA/λ(which shifts the diffraction spectrum to position the +2 diffraction order at the edge of the entrance pupil), doubling the theoretical resolution to d=λ/(2NA). Regardless of whether single-photon or two-photon exposure is utilized, the resolvable pitch for the exposure dose of adjacent projection light fields remains at the critical value of d=λ/(2NA), again limited by the minimum spacing from adjacent light intensity superposition, as depicted in Figure S8(c,e). Consequently,

d=λ/(2NA) defines the Sparrow criterion for parallel projection lithography under off-axis illumination conditions.

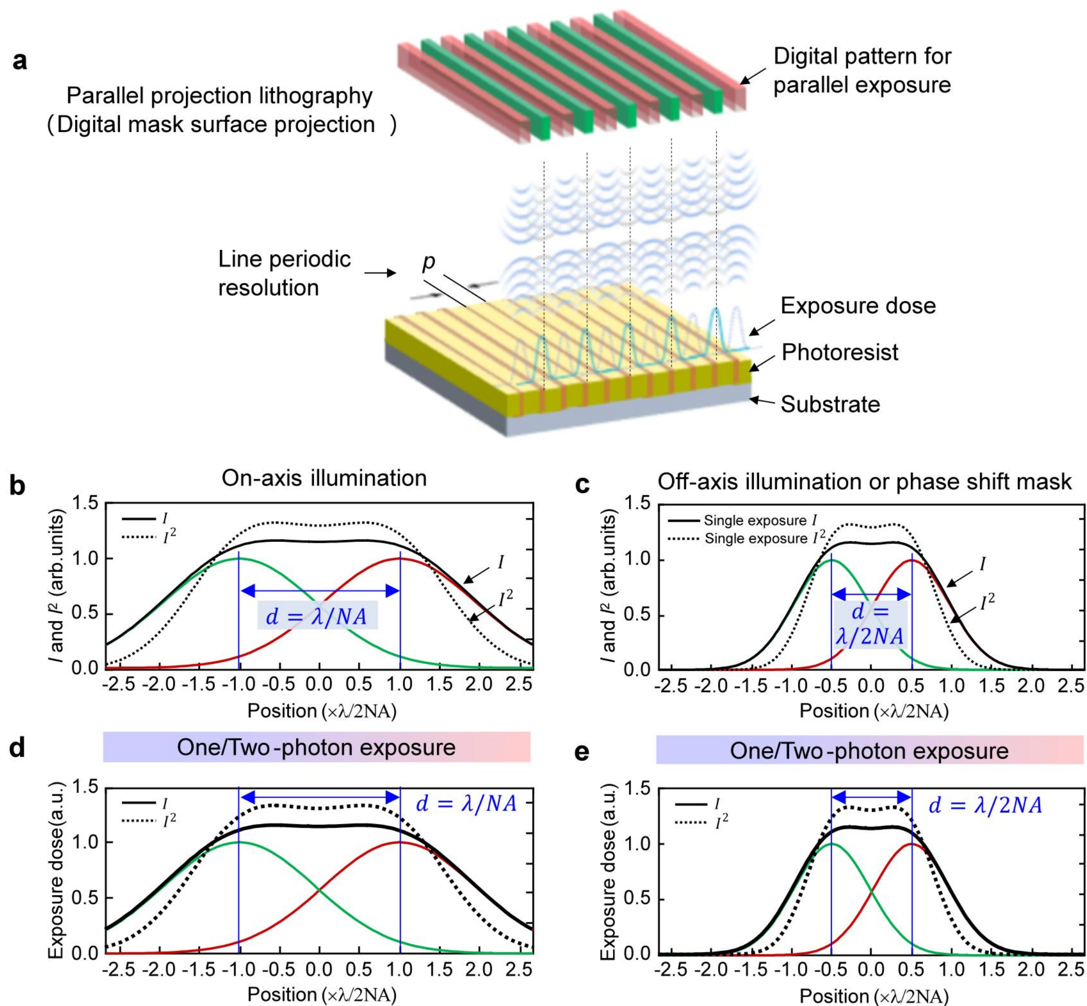

Figure S8 (a) Schematic diagram of parallel projection lithography; (b,c) Calculated focal intensity distribution for single exposure under off-axis illumination and off-axis illumination (or phase shift mask), respectively; Lateral profiles of I (solid line) and I^2 (dotted line) correspond to one-photon exposure and two-photon exposure, respectively. (d,e) Critical lateral distance for one/two-photon single exposure under off-axis illumination and off-axis illumination (or phase shift mask), respectively.

The digital mask projection lithography system discussed in this manuscript uses a collimated ultrafast laser beam aligned parallel to the optical axis, equivalent to the illumination of an object point at infinity on-axis. This setup corresponds to “the general Sparrow criterion” for parallel projection lithography with the phase shift mask, where d=λ/2NA. In our experiments, we used a laser with a center wavelength of 517 nm and an objective lens with an NA of 1.40, yielding a theoretical line pitch resolution of

approximately ~180 nm. Thus, a single exposure cannot achieve a line array pattern with a period of 235 nm (corresponding to 3 pixels). However, by using double exposure (with a single-exposure pattern resolution of 314 nm, equivalent to 4 pixels, which adheres to the Sparrow criterion), we obtained clear, distinguishable exposure results, as shown in Figure S16 of the manuscript.

Supplementary Note 7. Magnification error and calibration of projection objective system

Figure S9 shows the exposure result of the LCOS-SLM loaded with 128-pixel black and white squares under pure amplitude modulation. The grayscale of the black squares in the loaded pattern is 0, the grayscale of the white squares is 255, the power behind the objective lens is 2.48 mW, and the exposure time is 20 s. The theoretical period length of the 128-pixel black and white squares behind the 100× objective lens is 20.48 μm, and the experimental period length is 20.17 μm. The actual length is smaller than the theoretical length, indicating that the actual magnification of this system is greater than 100 times, about 102× times.

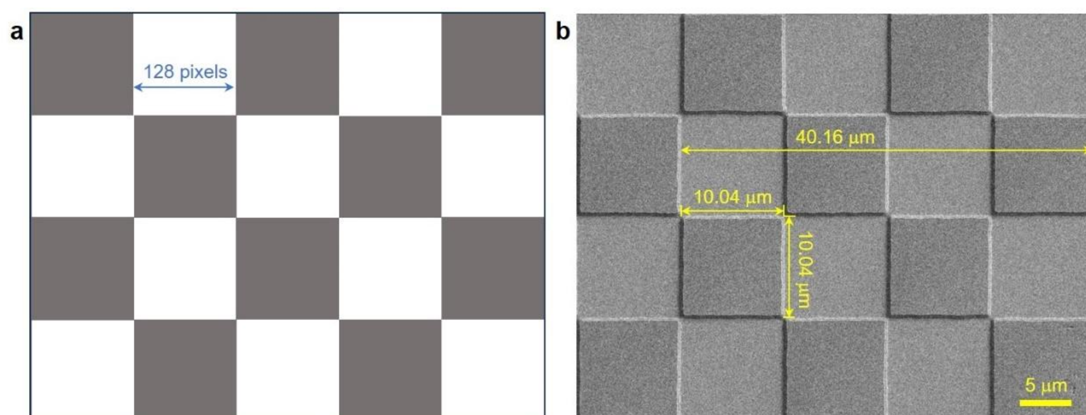

Figure S9 (a) Amplitude-only modulation digital mask layout; (b) SEM image of the calibration pattern.

Supplementary Note 8. Simulation and experimental results of dense pattern by pure phase modulation

Figure S10 shows the optical field distributions after the objective lens (100×, NA = 1.40) under pure phase modulation for dense patterns with half-pitches ranging from 1 to 10 pixels. Taking the case of a half-pitch of 1 pixel as an example, the phase-type LCOS-SLM is loaded with vertical lines having a width of 1 pixel and a spacing of 1 pixel. The lines are assigned to a grayscale value of 255, corresponding to a phase delay of π, while the spaces are assigned a grayscale value of 0, corresponding to a phase delay of 0. Thus, from the perspective of the loaded pattern, the full period is 2 pixels, and the half-period is 1 pixel. As shown in Figure S10, the use of the half-pitch definition arises because the optical fields corresponding to phase delays of π and 0 are essentially identical, except at the phase transition boundaries where destructive interference leads to dark regions. This optical field distribution is very similar to that produced by amplitude modulation. Therefore, from the perspective of the resulting optical field distribution, the effective fringe period is half of the period defined by the loaded pattern.

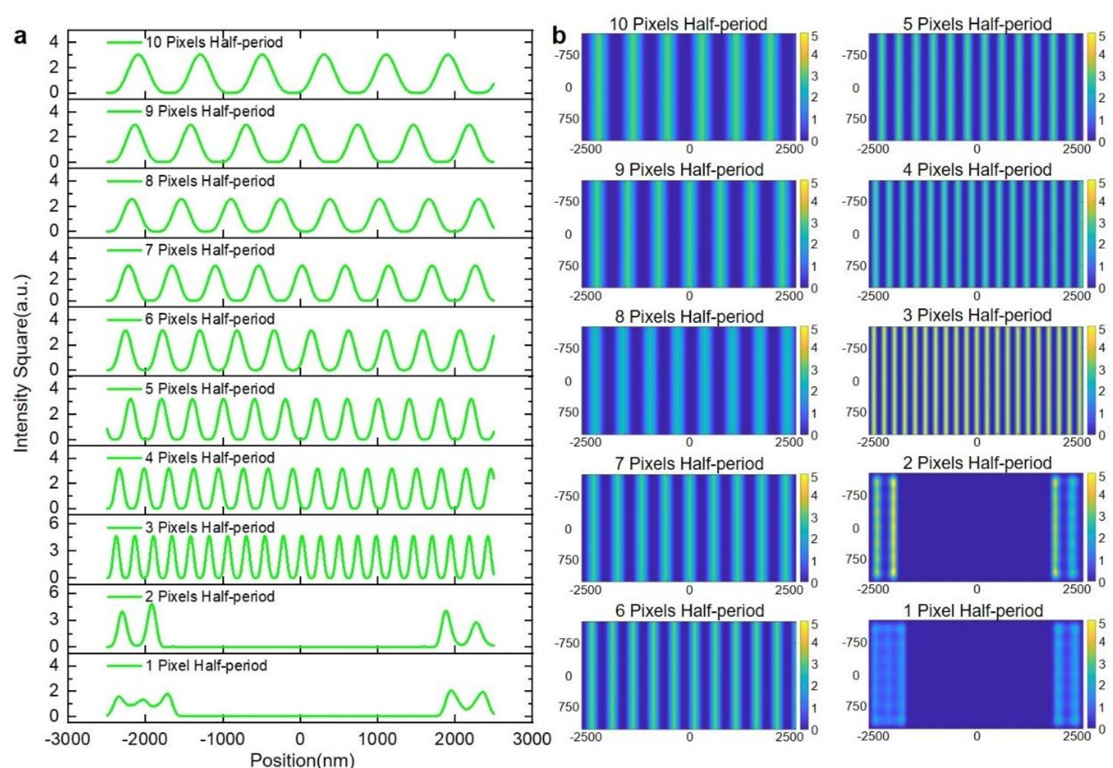

Figure S10 (a) 1D profile curve and (b) 2D spatial distribution of the projected light

intensity of the pure phase modulation “digital mask” from 1 to 10 pixels half-pitch.

In the case of pure phase modulation, the system's resolution limit corresponds to a half-pitch of 3 pixels. When the half-pitch is 1 or 2 pixels, the optical energy concentrates at the edges, with no significant field present in the center, making it impossible to form distinguishable structures. For pure amplitude modulation, the resolution limit is a full period of 5 pixels; when the period is less than 5 pixels (such as 3 or 4 pixels, as shown in Figure 3), the patterns also become unresolvable. This indicates that for both pure phase modulation and pure amplitude modulation, patterns with periods less than or equal to 4 pixels cannot be reliably resolved in exposure.

Figures S9 and S10 present the comparison between simulation and experimental results under pure phase modulation with half-pitches ranging from 1 to 10 pixels. In the images loaded onto the phase-type LCOS-SLM, the background has a grayscale value of 0, while vertical lines with a grayscale value of 255 are arranged according to different periods. In the experimental results, the observed lines can be categorized into two types: one corresponds to lines with a phase delay of 0.8773π, which, due to the phase conflict with the background, appear as complete and well-defined structures; the other corresponds to the background regions with a phase delay of 0, where the lines partially merge with the background at their ends but maintain complete structures in their central regions, as shown in Figure S10(b). The incident laser power was set at 4.12 mW with an exposure time of 35 seconds. The experimentally achieved resolution limit matches the simulations, with a half-pitch limit of 3 pixels. The measured periods in experiments show excellent agreement with the simulation results.

Regarding the linewidth, under identical conditions, the linewidths obtained by pure phase modulation are broader than those from pure amplitude modulation. For example, for a two-pixel-wide line with an 8-pixels period, the linewidth achieved by pure amplitude modulation is 167 nm (as shown in Figure 3), whereas the linewidth achieved by pure phase modulation with a 4-pixel half-period is 270 nm, despite the similar period size. The higher optical intensity observed in pure phase modulation compared to pure amplitude modulation is attributed to the fact that, in pure amplitude modulation with an 8-pixel

period, only 2 pixels contribute to the output light intensity, while in pure phase modulation with an 8-pixel half-period, all 8 pixels contribute to the output. Although in the experimental results the linewidths for regions with phase 0 and phase π are not perfectly identical, their periods remain equal, and the center-to-center spacing between adjacent lines in each case corresponds precisely to half of their respective period, which is consistent with theoretical calculations.

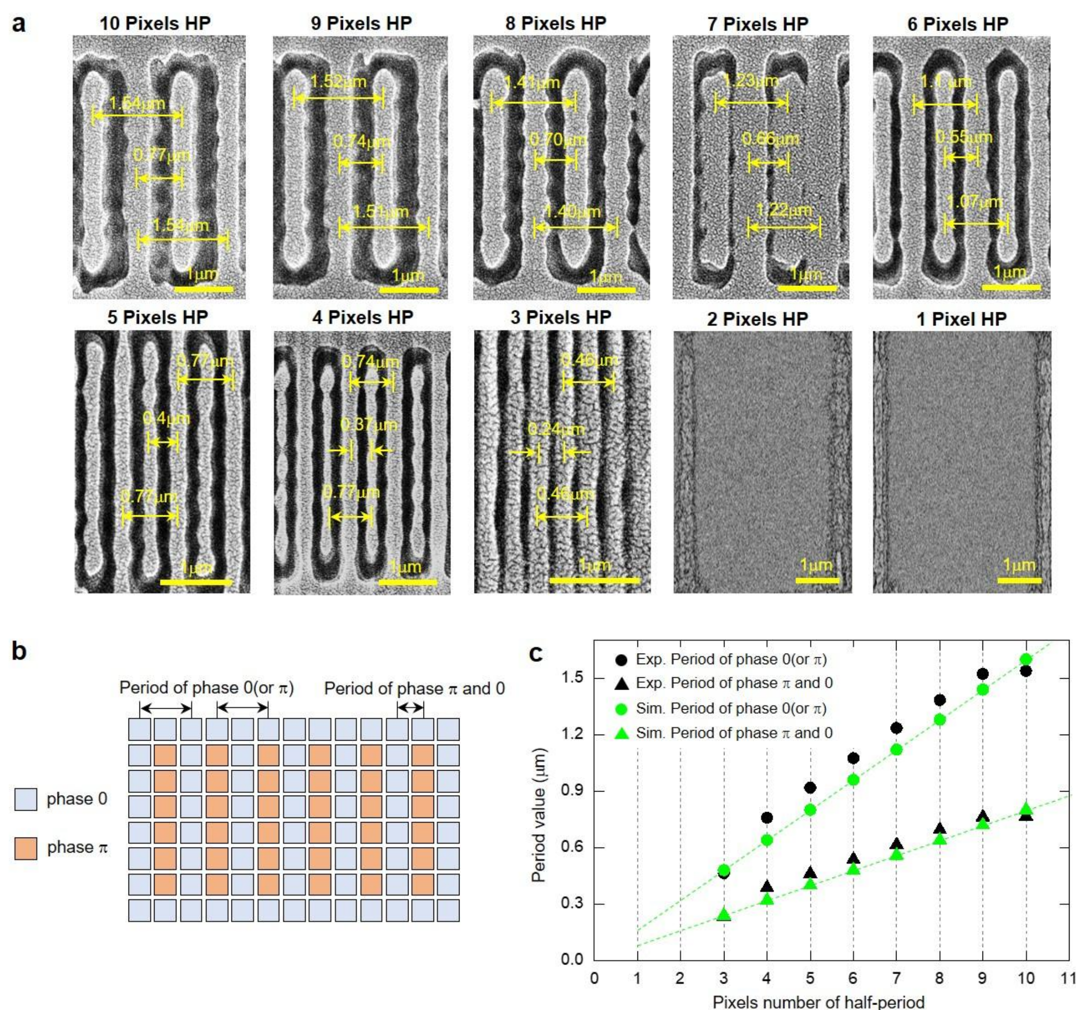

Figure S11 (a) Experimental results under pure phase modulation with a half-cycle of 1 to 10 pixels; (b) Schematic diagram of the 0 and pi phase pixel layout of the pure phase modulation "digital mask"; (c) Comparison of theoretical and experimental pitch value under pure phase modulation with a half-pitch of 1 to 10 pixels.

Although pure phase modulation can generate patterns similar to those produced by amplitude modulation, under identical experimental conditions, the linewidths obtained with pure phase modulation are significantly larger. Excessive exposure doses, combined

with the diffusion effects of the photoresist, can lead to merging of adjacent lines, thereby degrading the contrast of the exposed patterns.

More importantly, amplitude modulation can easily generate complex patterns by directly controlling light intensity, whereas pure phase modulation is fundamentally limited, as it relies on phase conflicts to induce intensity variations. For example, in this study, amplitude modulation successfully produced complete bright and dark stripe structures, while in pure phase modulation, the lines corresponding to the phase 0 regions could not exist independently. During negative photoresist exposure, the dark-field regions of the optical field form ring-like structures, as shown in Figure S11(a,b).

Supplementary Note 9. Linewidth control of digital phase-shift mask lithography

In addition to reducing the line spacing resolution (resolution) of a single exposure to near the diffraction limit, it is also necessary to consider controlling the line width (i.e., Critical Dimension, CD). Lithographic resolution is generally expressed as R/CD=k_1λ/NA, which has two implications. First, strictly speaking, R=k_1λ/NA represents the line-spacing resolution (as the reviewer noted as "the resolvability of two-point sources"), equivalent to half the smallest resolvable pitch of two adjacent line patterns (half-pitch). Second, in traditional lithography processes, the photoresist pattern is typically required to have a width-to-gap ratio of 1:1, where the width corresponds to the CD. To achieve this 1:1 width-to-gap ratio in resolvable pattern fabrication, the exposed linewidth CD must be controlled to be pitch/2, which gives CD=width=gap=HP=k_1λ/NA, thus expressing the linewidth resolution. Therefore, the lithographic resolution R/CD=k1λ/NA can describe both the linewidth limit and the pitch limit.

Lithography resolution:

$$R/CD = k_1 \frac{\lambda}{NA}$$

~ R (HP, half pitch) k_1≥0.25

~ CD (width : gap=1:1)

Width: the minimum width of line

Pitch: the distance of adjacent lines

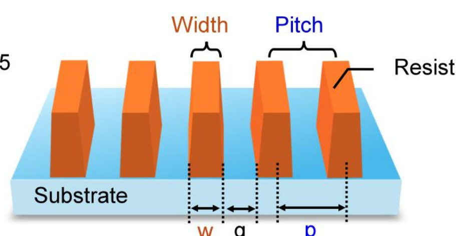

Figure S12 Definition of photolithography resolution (w: Width; g: Gap; p: Pitch).

From the simulation results in Figure 4 (d), we can see that the line width or CD of the dense pattern can be controlled by precise exposure dose changes. When the exposure conditions are Figure S13 (a) power 2.4 mW, exposure time 75 s; Figure S13 (b) power 2.4 mW, exposure time 65 s; Figure S12 (c) power 2.4 mW, exposure time 55 s, the obtained dense pattern line widths are ~100 nm, ~80 nm, ~60 nm. Therefore, the width-to-gap ratio can be controlled relatively accurately at 1:1 or even lower to meet the preparation requirements of semiconductor chips or photonic devices.

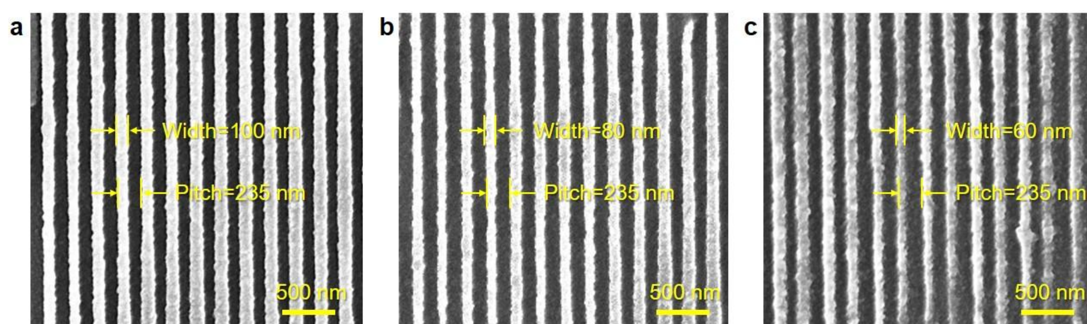

Figure S13 Linewidth or CD control of dense pattern with the exposure conditions: (a) the power of 2.4 mW, the exposure time of 75 s; (b) the power of 2.4 mW, the exposure time of 65 s; (c) the power of 2.4 mW, the exposure time of 55 s.

Supplementary Note 10. Spatial spectrum analysis of modulation methods

This paper focuses on three modulation methods, namely pure amplitude modulation, alternating phase shift mask modulation, and attenuated phase shift mask modulation. Take the grating mask loaded in Figure S14 (a) as an example, where the width of the light-transmitting line is *d* and the grating period is *p*.

The binary amplitude modulation spectrum can be expressed as

$$F_{BM} = \frac{(p-d)}{p}\sin c\,[f(p-d)] \cdot \sum_{n=-\infty}^{+\infty} \delta\left(f - \frac{n}{p}\right) \quad n = 0, \pm 1, \pm 2, \cdots \tag{S10}$$

The alternating phase shift mask modulation spectrum can be expressed as

$$F_{ALT} = \frac{(p-d)}{p}\sin c\,[f(p-d)]\sin(\pi f p) \cdot \sum_{n=-\infty}^{+\infty} \delta\left(f - \frac{n}{2p}\right) \quad n = 0, \pm 1, \pm 2, \cdots \tag{S11}$$

where the pupil coordinate is *f* and the diffraction order is *n*.

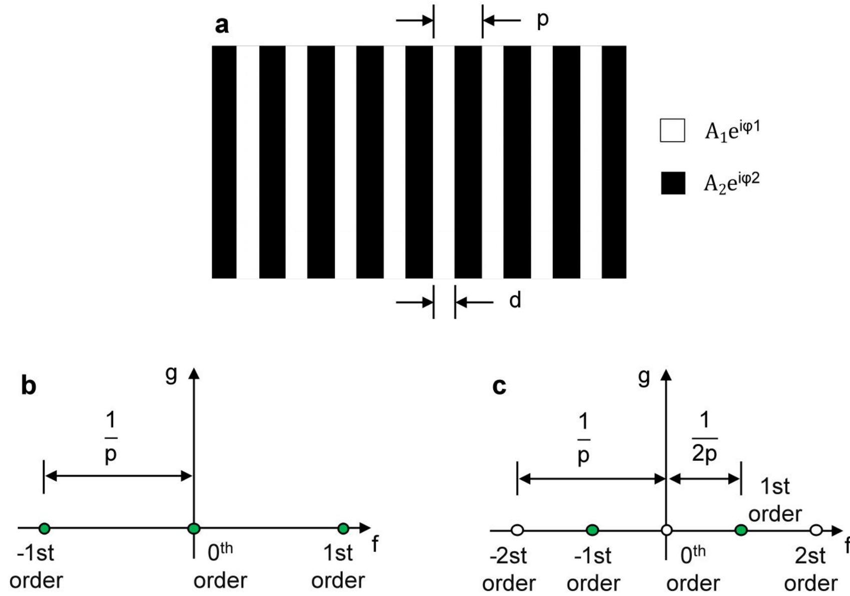

Figure S14 (a) Grating mask; (b) Binary amplitude modulation spectrum; (c) Alternating phase-shift mask modulation spectrum.

Compared with binary amplitude modulation, the spectrum period of alternating phase shift mask modulation is reduced to half of the original one; that is, the same spectrum width of alternating phase shift mask modulation can transmit more information. In addition, alternating phase shift mask modulation makes the 0th level and even-level

spectrum intensity 0, which increases the local contrast. These enable alternating phase shift mask modulation to improve resolution.

Supplementary Note 11. Light field simulation below the diffraction limit

The above experimental results show that the use of alternating phase-shift masks can improve the system resolution to 239 nm period, corresponding to the SLM loading period of 3-pixel images. Since the pattern generated by the SLM is arranged in pixels, the minimum period of the SLM loading image is 2 pixels, that is, 1 pixel width line, line interval 1 pixel. Figure S15 shows the corresponding simulation results. The simulation loading image is 200 pixels × 200 pixels, the middle 100 pixels × 100 pixels are loaded with 2-pixel vertical stripes, the amplitude and phase grayscale loaded in the adjacent area are both 0, and no light field control is performed.

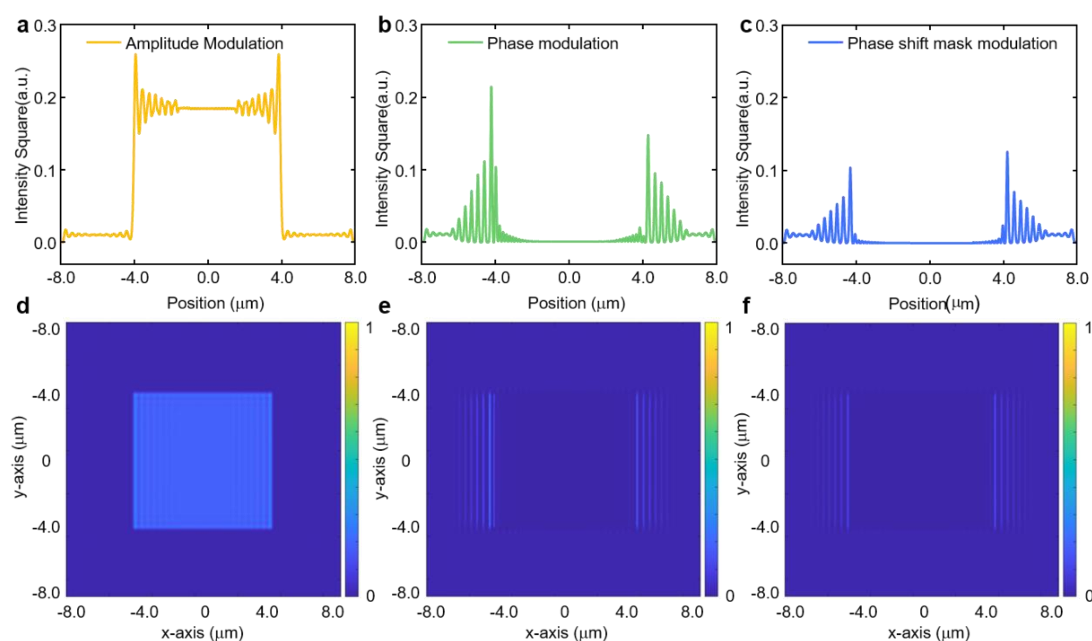

Figure S15 Light field intensity distribution of 1-pixel width line and 2-pixel period pure amplitude modulation (a), pure phase modulation (b) and alternating phase shift mask modulation (c).

Under pure-amplitude modulation, there is a light field fluctuation at the edge of the middle figure, and the light intensity contrast in the middle area is extremely low, and the stripe structure cannot be distinguished. Pure phase modulation and alternating phase shift mask modulation both transfer the middle light field to both sides, and the integral area of the light field curves of the three, that is, the total outgoing light intensity, is 1611, 189, and 136, respectively. This is because after using phase modulation for the amplitude 2-pixel period structure, the light field energy will be distributed to higher

diffraction orders, and these high-order diffraction order light fields cannot enter the objective lens. Alternating phase shift mask modulation is affected by the phase modulation limit. The minimum resolution that can be achieved in this system is a 3-pixel period structure, that is, a 239 nm period. For structures smaller than this period, alternating phase shift mask modulation causes the light field to gather on both sides of the structure, and the desired structure cannot be obtained.

Supplementary Note 12. Exposure demonstration of complex graphic layout

Here, we use the alternating phase shift mask technique to expose complex patterns. Figure S16(a) shows a negative map of China with dense line patterns (width: pitch = 3:4). The exposure results show a line spacing resolution of 315 nm and a line width of 141 nm, see Figure S16(b). Figure S16(c) shows a positive map of China with dense line patterns (width: pitch = 3:4). The exposure results show a line spacing resolution of 315 nm and a line width of 200 nm, see Figure S16(b). The difference in line width is caused by uneven energy in different areas of the exposure field. The experimental conditions for exposure are a laser power of 5.3 mW and an exposure time of 50 s.

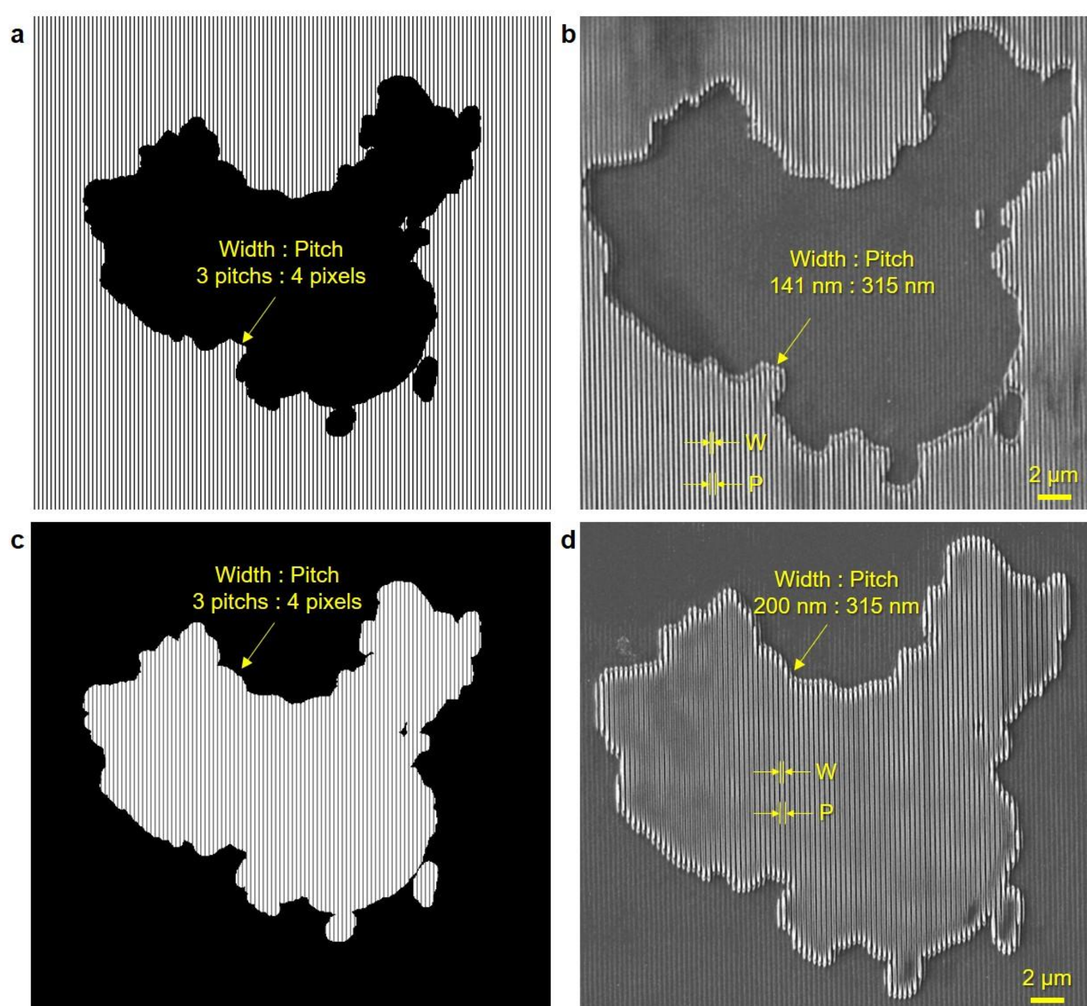

Figure S16 Alternating phase-shift mask exposure of complex layouts: (a) negative engraving of the map of China and (b) SEM image of the exposure result, (c) positive engraving of the map of China and (d) SEM image of the exposure result.

Supplementary Note 13. Exposure demonstration of metal layer patterns in chip layout

Based on the ordered layout design in Figure 5 (a) or Figure S17 (a), the amplitude mask loaded in the SLM is composed of a relatively dense small-period line array and a relatively sparse large-period line array. The small-period line array is set to 2 pixels wide and 4 pixels period, and the large-period line array is set to 2 pixels wide and 8 pixels period. The light field distribution of the small-period dense array pattern in the focal plane is indistinguishable, while the light field distribution of the large-period dense array pattern in the focal plane is distinguishable, as shown in Figure S17 (a), which is consistent with the theoretical and experimental analysis in Figure 3. Similarly, from the focal plane light field simulation of the unordered layout in Figure S17 (b) (which can be considered as a quasi-periodic dense pattern with a period of 4 pixels), it can be seen that the simulated light field distribution of the loaded PSM phase-shift mask is distinguishable, while the comparison of the pure amplitude mask modulation projection light field is still indistinguishable.

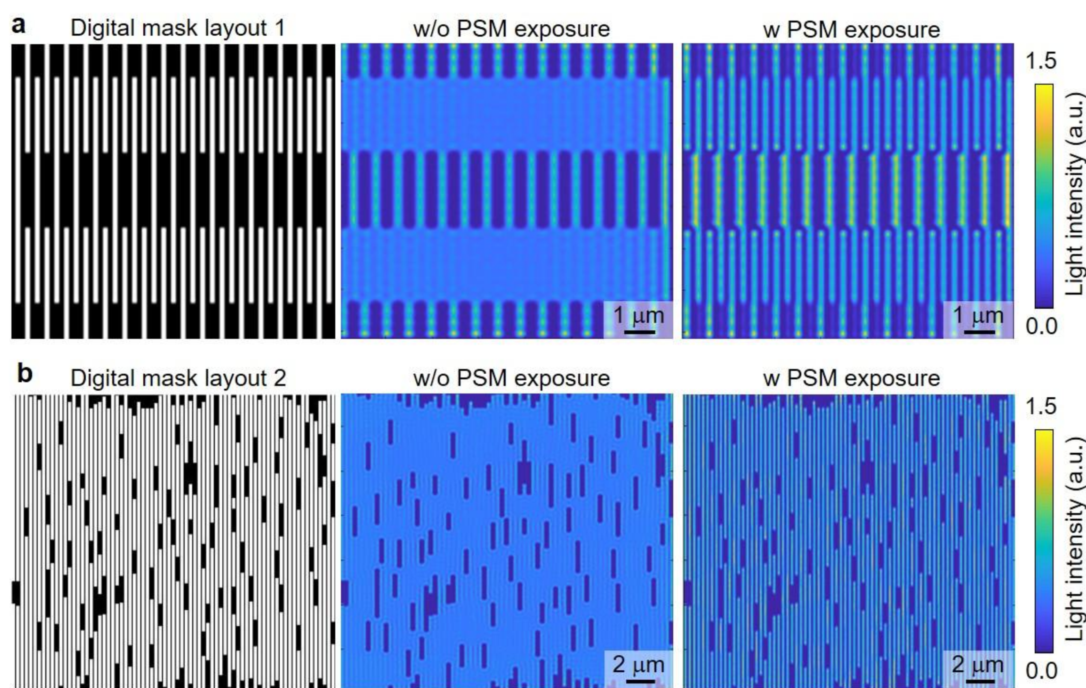

Figure S17 Comparison of simulation results for chip metal layer layout. (a) Digital mask and SEM images of the ordered layout. (b) Digital mask and SEM images of the unordered layout.

For the exposure of the ordered pattern in Figure S18 (a), even if the PSM digital lithography technology is used, the exposure dose of the periodic line array pattern in the cross region will be too high due to the proximity effect. The alternating phase shift mask technology is combined with the amplitude grayscale modulation, and the exposure pattern line width in different dense patterns is kept consistent through local light intensity grayscale modulation. As shown in Figure S18, the grayscale value loaded by the amplitude mask corresponding to the small period line array (i.e., the cross region, 2 pixels wide and 4 pixels period) and the large period line array pattern (2 pixels wide and 8 pixels period) is 255, and the light field intensity of the 4-pixel period line array is inconsistent with that of the 8-pixel period line array.

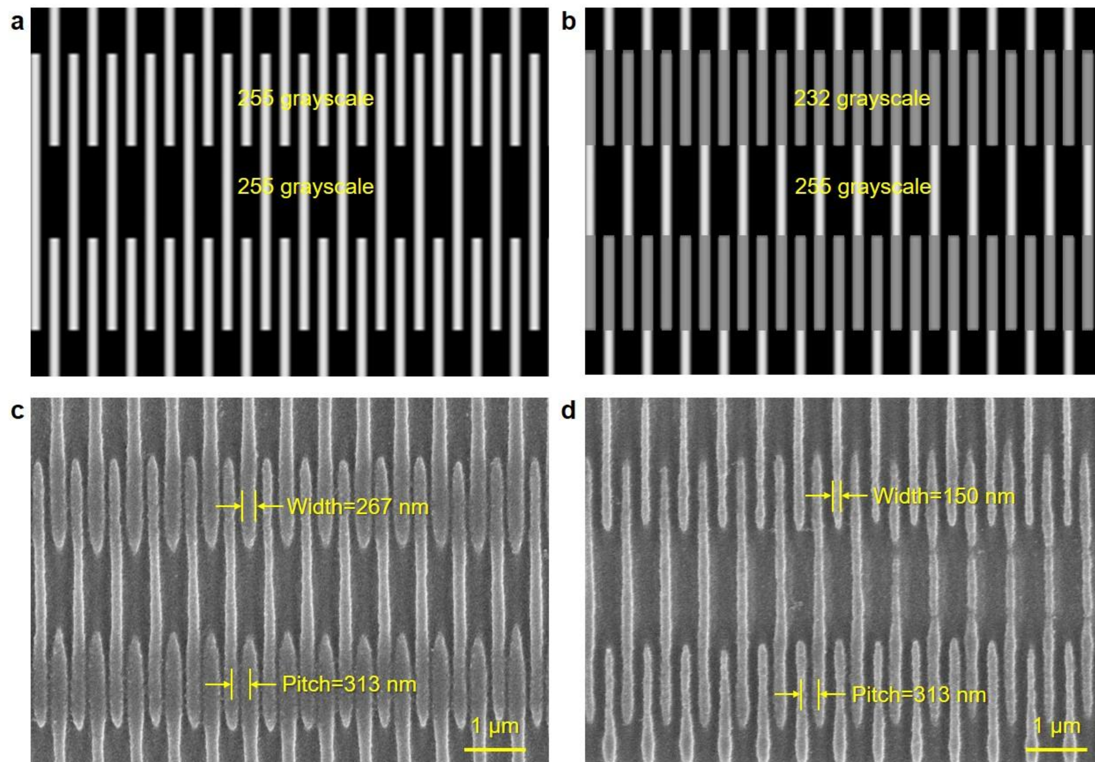

Figure S18 Comparison of experiment results for phase-shift mask technology with amplitude grayscale modulation. (a) Uniform amplitude modulation; (b) Amplitude grayscale modulation.

As shown in the light intensity contour distribution diagram of Figure S17 (a), under the exposure conditions of 1.6 mW and 260 s, the line width of the small period line array in the dense area is 267 nm, which is higher than the line width of the large period line array (Figure S18(c)). Furthermore, we combined the alternating phase shift mask

technology with amplitude grayscale modulation, keeping the phase mask unchanged, setting the 4-pixel periodic line of the amplitude mask to 232 grayscale, and keeping the 8-pixel periodic line to 255 grayscale (Figure S18(b)). Compared with the binary amplitude mask (Figure S18(a)), the grayscale amplitude mask reduces the line width difference caused by different periods. As shown in Figure S18(d), the line width of the small-period line array in the dense area is basically the same as the line width of the large-period line array. It can be seen that the amplitude grayscale modulation can effectively improve the process window. At the same time, it also proves that the complex amplitude modulation system we have realized can modify and optimize the mask at multiple angles according to different target graphics.

Supplementary Note 14. Double exposure of PSM digital lithography

Based on the single PSM digital lithography process, double exposure can be used to further improve the pitch resolution. Taking the 2-pixel periodic line pattern as an example, according to the theoretical analysis in Figure 3, the periodic line pattern cannot be distinguished even if PSM is used for exposure. We first decompose the 2-pixel periodic line pattern into two 4-pixel periodic line patterns, as shown in Figure S19(a). We calculate the projection light field distribution I_1 and I_2 of the two 4-pixel periodic line patterns, respectively.

It is important to note that the resolution enhancement in this system arises from two complementary mechanisms with distinct physical origins. The phase-shifting mask (PSM) introduces controlled phase differences between adjacent pixels, resulting in destructive interference that suppresses the intensity between neighboring features and effectively increases the spatial frequency content of the optical field, which primarily governs the pitch resolution. The two-photon polymerization (TPP) process, on the other hand, relies on the nonlinear thresholding behavior of the photoresist, where polymerization occurs only in regions exceeding a certain intensity. This nonlinear effect sharpens feature boundaries and allows the line width to be smaller than the diffraction-limited spot. In other words, while PSM defines the spacing between features, TPP further refines the feature size within each high-intensity region.

Considering that the 517 nm exposure uses a two-photon absorption photoresist physical model, the effective exposure dose is proportional to the light intensity squared, $D \propto I^2$. Therefore, we superimpose the two projection light fields to obtain the total exposure dose $D \propto I_1^2 + I_2^2$. The two-dimensional cross-sectional distribution diagram is shown in Figure S19(c), where the green representation corresponds to the superposition of the two exposures. The SEM photo of the exposed structure is shown in Figure S19(b), obtained under the exposure conditions of P = 1.6 mW and T = 260 s. The resulting line width is about 100 nm, the line period is 158 nm, and the line morphology contrast is reduced, which is also reflected in the theoretical calculation results shown in Figure S19(c).

This analysis highlights the complementary roles of PSM and TPP in the double-exposure process: PSM enables sub-diffraction pitch resolution, while TPP allows further refinement of linewidth, providing a comprehensive understanding of the mechanisms underlying the observed feature sizes and contrasts.

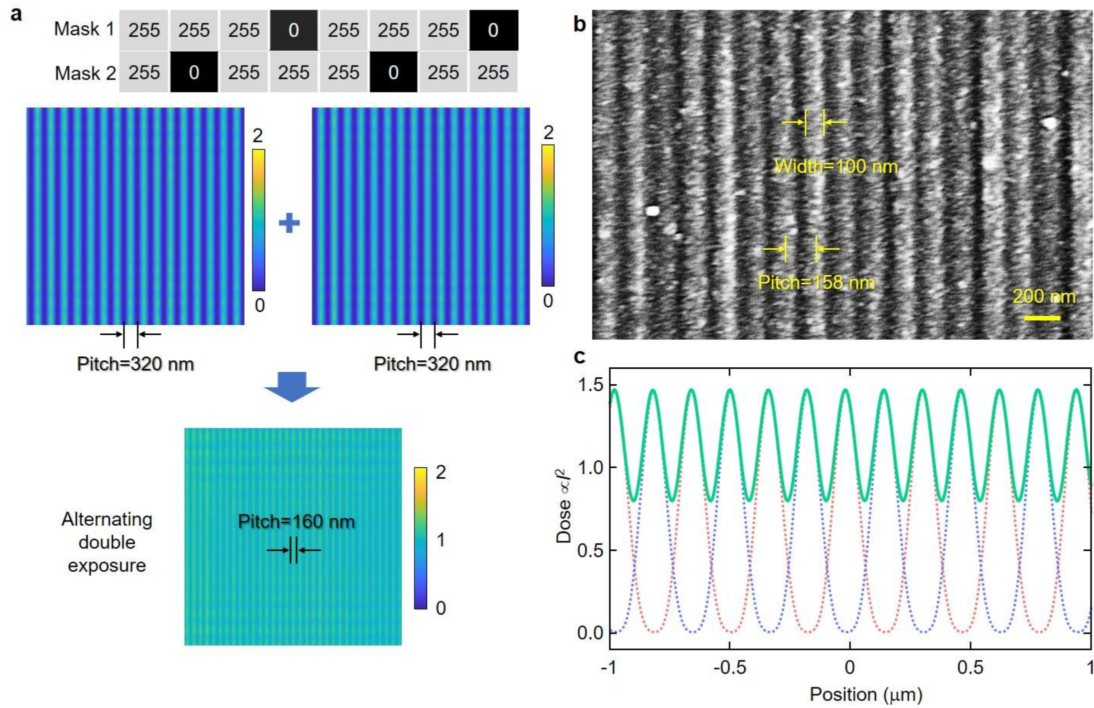

Figure S19 (a) The 2-pixel periodic dense pattern is split into two 4-pixel periodic dense patterns and their corresponding light field simulation; (b) SEM image of double exposure; (c) simulation result of exposure dose superposition of two exposures.

Supplementary Note 15. Comparison of process node parameters between PSM digital lithography and traditional lithography

We listed the lithography pattern characteristic parameters of traditional lithography at the N180 ~ N2 process nodes, see Table S3. At the same time, we equated the limit resolution achieved by PSM digital lithography technology with the existing standard process node parameters. Its 312nm-pitch is equivalent to meeting the chip design rules of the N130 process node; 235 nm-pitch is equivalent to meeting the chip design rules of the N90 process node. Therefore, the single-exposure PSM digital lithography technology we studied can achieve the N90 node process. By introducing a multiple exposure strategy as shown in Figure S19, 158 nm-pitch dense pattern exposure can be achieved, which is equivalent to meeting the chip design rules of the N45 process node. Further use of a 400 nm light source is expected to reduce the dense pattern pitch to 90nm, achieving N28 process node chip layout exposure that meets advanced processes.

Table S3 Comparison of process node parameters

Node	Metal pitch(nm)	Lamda (nm)	NA	k1	Process method
N180	460	248	0.63	0.584274	248 nm Dry Lithography
N130	340	248	0.7	0.479839	
N90	240	193	0.75	0.466321	193 nm (DUV) Dry Lithography
N65	180	193	0.93	0.433679	
N45	160	193	1.2	0.497409	193 nm (DUV) Immersion lithography (Water)
N40	100	193	1.35	0.349741	
N32	90	193	1.35	0.314767	
N28	90	193	1.35	0.314767	
N22	80	193	1.35	0.279793	
N20	64	193	1.35	0.223834	193 nm (DUV) immersion lithography + multiple patterning
N14	64	193	1.35	0.223834	
N10	44	193	1.35	0.153886	
N7	40	193	1.35	0.139896	
N5	30	13.5	0.33	0.366667	13.5 nm (EUV) Lithography
N3	22	13.5	0.33	0.268889	
N2	16	13.5	0.55	0.325926	
Equ. N130[(1)]	312	517	1.40	0.422437	PSM digital lithography (517nm)

Equ. N90[2]	235	517	1.40	0.318182	
Equ. N45[3]	158	517	1.40	0.213926	PSM digital lithography (517nm) + multiple exposure
Equ. N28[4]	90	517	1.40	0.121857	PSM digital lithography (400nm) + multiple exposure

(1), (2), (3), and (4) represent the lithography characteristic parameters of equivalent process nodes N130, N90, N45, and N28, respectively.

Supplementary References:

[1] Gregory D A, Kirsch J C, Tam E C. Full complex modulation using liquid-crystal televisions[J]. Applied Optics, 1992, 31(2): 163-165.

[2] Van Putten E G, Vellekoop I M, Mosk A P. Spatial amplitude and phase modulation using commercial twisted nematic LCDs[J]. Applied optics, 2008, 47(12): 2076-2081.

Mendoza-Yero O, Mínguez-Vega G, Lancis J. Encoding complex fields by using a phase-only optical element[J]. Optics letters, 2014, 39(7): 1740-1743.

[3] Goorden S A, Bertolotti J, Mosk A P. Superpixel-based spatial amplitude and phase modulation using a digital micromirror device[J]. Optics express, 2014, 22(15): 17999-18009.

[4] Han W, Yang Y, Cheng W, et al. Vectorial optical field generator for the creation of arbitrarily complex fields[J]. Optics express, 2013, 21(18): 20692-20706.

[5] Zhu L, Wang J. Arbitrary manipulation of spatial amplitude and phase using phase-only spatial light modulators[J]. Scientific reports, 2014, 4(1): 7441.

[6] Leportier T, Park M C, Kim T. Numerical alignment of spatial light modulators for complex modulation in holographic displays[J]. Journal of Display Technology, 2016, 12(10): 1000-1007.

[7] Fischer J, Wegener M. Three-dimensional optical laser lithography beyond the diffraction limit[J]. Laser & Photonics Reviews, 2013, 7(1): 22-44.

[8] Andreas Erdmann. Optical and EUV Lithography: A Modeling Perspective[M]. Publisher. SPIE; Publication date. March 2, 2021.

[9] Schellenberg F M. Resolution enhancement technology: the past, the present, and extensions for the future[C]//Optical Microlithography XVII. SPIE, 2004, 5377: 1-20.

[10] Sparrow C M. On spectroscopic resolving power[J]. Astrophysical Journal, vol. 44, p. 76, 1916, 44: 76.

[11] Masters B R, Masters B R. Abbe’s theory of image formation in the microscope[J]. Superresolution optical microscopy: The quest for enhanced resolution and contrast, 2020: 65-108.

[12] Shibuya M. Resolution enhancement techniques for optical lithography and optical

imaging theory[J]. Optical Review, 1997, 4: 151-160.

[13] Levenson M D, Viswanathan N S, Simpson R A. Improving resolution in photolithography with a phase-shifting mask[J]. IEEE Transactions on electron devices, 1982, 29(12): 1828-1836.

[14] Zhao Y, Dong L, Li Z, et al. LIC-CGAN: fast lithography latent images calculation method for large-area masks using deep learning[J]. Optics Express, 2024, 32(23): 40931-40944.

[15] Li Z, Dong L, Ma X, et al. Decomposition-learning-based thick-mask model for partially coherent lithography system[J]. Optics Express, 2023, 31(12): 20321-20337.

[16] Lanza M, Pazos S, Aguirre F, et al. The growing memristor industry[J]. Nature, 2025, 640(8059): 613-622.

[17] Moon J H, Jeong E, Kim S, et al. Materials quest for advanced interconnect metallization in integrated circuits[J]. Advanced Science, 2023, 10(23): 2207321.

[18] Raza A, Saeed Z, Aslam A, et al. Advances, application and challenges of lithography techniques[C]//2024 5th International Conference on Advancements in Computational Sciences (ICACS). IEEE, 2024: 1-6.